Mice wiggle a wheel to boost the salience of low visual contrast stimuli

Naureen Ghani and The International Brain Laboratory

27 August 2025

Abstract

From the Welsh tidy mouse to the New York City pizza rat, movement reveals rodent intelligence. Akin to humans shaking a computer mouse to find the cursor on a screen, we show that head-fixed mice develop an active sensing strategy in a visual perceptual decision-making task (**The International Brian Laboratory, 2021**). We demonstrate that mice wiggle a wheel that controls the movement of a stimulus during low visual stimulus contrast trials. When animals wiggle, the low visual stimulus contrast accuracy increases by 6.0% (Pearson correlation, $r = 0.900, p = 0.038, N = 5$ group means computed from 213 mice). Moreover, mice wiggle the wheel at a speed that corresponds to a visual stimulus temporal frequency (11.52 ± 2.45 Hz) demonstrated to maximize contrast sensitivity in a Go/No-Go task (**Umino et al, 2018**). These findings suggest that mice wiggle a wheel to boost the salience of low visual contrast stimuli.

Highlights

- Mice developed an active sensing strategy in a visual perceptual decision-making task while head-fixed.
- Mice wiggled a wheel that controlled the movement of a visual stimulus as a function of contrast.
- The median wiggle speed associated with visual temporal contrast sensitivity closely matched the flicker frequency at which mice performed best in a Go/No-Go task (**Umino et al, 2018**).
- Decoding stimulus identity from neural activity improved with longer wiggles in midbrain and thalamic regions, including the superior colliculus.

1 Introduction

Active sensing is the use of movement to enhance sensory perception. It is well-studied in freely moving worms (Kato et al, 2015), flies (Fenk et al, 2022; Wang et al, 2022), and rats (Kurnikova et al, 2017; Liao and Kleinfeld, 2023). Sensing actions often involve moving the stimulus into a region of high acuity (Zhaoping, 2019). For example, visual active sensing in humans and monkeys relies on the fovea, which is the high-acuity region of the retina. Humans use eye fixations to improve discrimination of high spatial frequency stimuli (Rucci et al, 2007) and adapt microsaccades to improve visual acuity (Intoy and Rucci, 2020; Zhao et al, 2023). Similarly, head-fixed monkeys use eye saccades to sample a visual scene (Mitchell et al, 2014; Xiao et al, 2024; Singh et al, 2025). Since rats and mice are non-foveal, relatively little is known about visual active sensing in head-fixed rodents. One claim that motivates this work is that uninstructed movement dominates head-fixed mouse cortex-wide activity during a visual decision-making task (Musall et al, 2019).

Beyond active sensing, the interaction of vision and movement in locomotion is well-studied in head-fixed mice. Mouse primary visual cortex (V1) encodes locomotion (Niell and Stryker, 2010; Keller et al, 2012; Ayaz et al, 2013; Saleem et al, 2013; Stringer et al, 2019) and locomotion enhances neural encoding of visual stimuli in mouse V1 (Dadarlat and Stryker, 2017; Dipoppa et al, 2018). The majority of mouse V1 neurons are modulated by head movements (Meyer et al, 2018) in a luminance-dependent manner (Bouvier et al, 2020; Guitchounts et al, 2020). Mouse eye saccades tend to be coupled to head movements (Parker et al, 2022) and while head-fixed mice do saccade, these movements are likely not predominantly visually driven (King et al, 2023).

We believe that head-fixed mice develop an active sensing strategy while performing a visual decision-making task. Our hypothesis is that mice wiggle a wheel that controls the movement of a visual stimulus when sensory information is limited. Wiggling transforms a spatial frequency into a temporal frequency, which boosts the salience of the visual stimulus, as the mouse visual system is particularly sensitive to temporal changes (Gulbinaite et al, 2024).

We test this hypothesis using large-scale data analysis approaches across and within mice. We ask (1) does the low visual stimulus contrast accuracy increase with wiggles? This question is motivated by examples of visual accuracy gains with head-movement jitters (Fulvio et al, 2021) and retinal-image jitters (Palmisano et al, 2009;

Watson et al, 2012) in humans. (2) Are higher speed wiggles more accurate? This question is motivated by studies that demonstrate improvement in psychophysical performance with higher speed visual stimuli in humans (Rolfs et al, 2025) and monkeys (Huang et al, 2024). (3) What proportion of mice benefit from wiggles? This addresses the null hypothesis that wiggles are irrelevant to performance. Motivated by classic examples of active sensing in rodents such as whisking and sniffing, we used continuous and discrete metrics of wiggles to determine which mice benefit from an active sensing strategy.

1.1 Mice used a wheel to center a visual stimulus for sugar-water reward.

We analyzed behavioral data from 213 mice that performed a visual perceptual decision-making task while head-fixed (**Figure 1a**). Mice were trained to use a miniature steering wheel that controlled the movement of a visual stimulus (The International Brain Laboratory, 2021). When mice moved the wheel for a total of 8.75 millimeters to center the visual stimulus, they earned sugar-water reward (**Figure 1b**). With a visuo-motor gain of 4 visual degrees per millimeter of wheel movement, this 8.75 mm corresponded to 35 visual degrees of stimulus movement (8.75 mm $\times$ 4 visual degrees/mm = 35 visual degrees).

We used a shaping protocol to gradually train mice to perform the visual decision-making task at increasingly difficult contrast levels. Mice began with trainingChoiceWorld sessions (left and right stimuli were presented with equal probability) containing only 100% and 50% contrast trials. When the proportion correct reached 70%, we consecutively added lower contrast trials: first adding 25% contrast, then adding 12.5% contrast while replacing 50% with 0% contrast trials, and finally adding 6.25% contrast trials. These final sessions with the full range of contrast levels (100%, 25%, 12.5%, 6.25%, and 0%) constituted the late-stage trainingChoiceWorld sessions used for analysis.

After learning the visual detection task, mice progressed to biasedChoiceWorld sessions (left and right stimuli were presented with unequal probability) (see Appendix 2 of The International Brain Laboratory et al, 2021 for details). When neural data was acquired during these biasedChoiceWorld sessions, we refer to them as ephysChoiceWorld sessions.

Our behavioral dataset consisted of three session types: 54.36% biasedChoiceWorld sessions (2761 sessions), 38.94% late-stage trainingChoiceWorld sessions (1978 sessions), and 6.70% ephysChoiceWorld sessions (340 sessions).

The probability of a left visual stimulus was manipulated in strictly alternating biased blocks for sets of $20-100$ trials (**Figure 1c**). A session consisted of (1) 90 trials in an unbiased block (50/50) followed by (2) $4-5$ left (80/20) and right (20/80) blocks. The independent variable was visual stimulus contrast, which ranged from high (1.0), intermediate (0.25 and 0.125), low (0.0625), and zero (0.0) (**Figure 1d**). Each trial had a variable quiescent period duration from 0.40 to 0.70 seconds (computed as 0.2 seconds + a duration drawn from an exponential distribution with a mean of 0.35 seconds, min and max of 0.20–0.50 seconds) (**Figure 1e**) (Appendix 2 of The International Brain Laboratory et al, 2021). The inter-trial interval was fixed at 0.5 seconds for correct trials and 2 seconds for error trials.

The reaction time distribution across mice ($3,329,275$ trials) was bimodal, which is how we defined 0.08 seconds as the threshold for a visual stimulus-triggered response (**Figure 1f**). We plotted reaction times between -0.20 and 0.50 seconds, which represents 86.10% of the data. This implies that the proportion of data not shown in **Figure 1f** is 13.90%, where the reaction time exceeded 0.50 seconds. During visual stimulus-triggered trials, the proportion of counterclockwise choices was a function of block (**Figure 1g**). Thus, mouse behavior was biased by blocks.

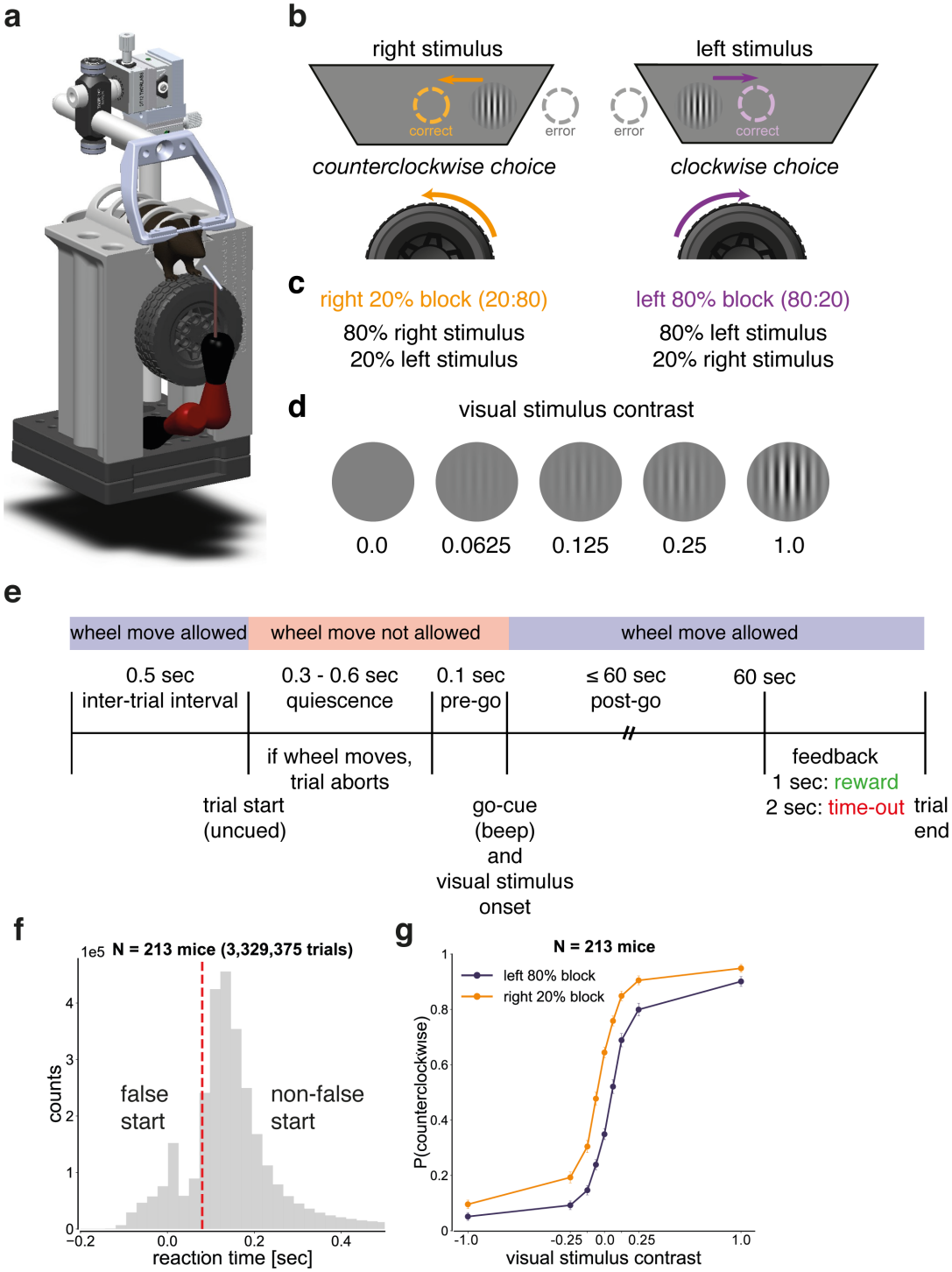

Figure 1: **Mice used a wheel to center a visual stimulus for reward.** **(a)** A head-fixed mouse used a miniature steering wheel (The International Brain Laboratory, 2021) to indicate choice. Schematic by: Florian Rau. **(b)** Mice turned the wheel counterclockwise for a right visual stimulus and clockwise for a left visual stimulus to earn sugar-water reward. Mice received negative feedback (a 2-second time-out with a gray screen) if the visual stimulus fell off the screen. **(c)** The task has a block structure. The **left 80% block** consisted of 80% left visual stimuli and 20% right visual stimuli (**80:20**). The **right 20% block** was the converse and consisted of 80% right visual stimuli and 20% left visual stimuli (**20:80**). **(d)** The independent variable was visual stimulus contrast: $[0.0, 0.0625, 0.125, 0.25, 1.0]$. **(e)** The task has a trial structure with a variable quiescent period duration ($0.4 - 0.7$ seconds) and a free-response period (60 seconds). **(f)** The reaction time distribution inclined at 0.08 seconds across $N = 213$ mice, which is the threshold for non-false starts (indicated by red dashed line). **(g)** The psychometric curves were dependent on visual stimulus contrast (one-way repeated measures ANOVA, **left 80% block:** $F = 982.3, p < 0.001$, **right 20% block:** $F = 1109.7, p < 0.001$) and block (one-way repeated measures ANOVA, $p < 0.05$) in non-false starts. Error bars represent the binomial proportion confidence intervals (CI).

2 Results

2.1 Wiggles are wheel movements with multiple changes in wheel direction.

To determine whether low visual stimulus contrast accuracy depends on wheel movement dynamics, we defined a discrete measure of directional changes. This metric is denoted as k, which quantifies the number of changes in wheel movement direction during a trial.

This was computed from wheel position data interpolated at 1000 Hz, which captured the general motion of the wheel with superimposed rapid directional changes. Directional changes were identified by counting zero crossings in the derivative of the position signal, which were points where the wheel velocity (in degrees per second) changed sign.

The wheel data in each mouse was stratified by k into one of five groups: (1) $k = 0$, (2) $k = 1$, (3) $k = 2$, (4) $k = 3$, and (5) $k \geq 4$.

k value	Movement pattern	Interpretation	Wiggle?
0	single-direction movement	ballistic, confident choice	No
1	one directional change	change-of-mind or near-ballistic	No
≥ 2	multiple directional changes	active sensing, change-of-mind, or disengagement	Yes

Table 1: Summary of wheel movement dynamics: k is the number of directional changes.

A trial with $k = 0$ directional changes is defined as a non-wiggle (**Figure 2a**). Such trials are examples of ballistic movements, which are high-velocity, high-acceleration movements done within a short period of time.

A trial with $k = 1$ directional changes is defined as a non-wiggle with one sign reversal (**Figure 2b**). Such trials could represent change-of-mind, which is a revision in the initial choice based on accumulated evidence (**Figure 1b**). An alternative explanation is that $k = 1$ directional changes are near-ballistic movements. To distinguish change-of-mind from near-ballistic, reaction time and wheel amplitude can be used. While near-ballistic movements will have fast reaction times ($0.1 - 0.2$ seconds) and small wheel amplitudes (below 2 degrees), change-of-mind trials will have longer reaction times indicative of deliberation ($0.4 - 0.5$ seconds) and greater wheel amplitudes (upwards of 2 degrees) indicative of evidence accumulation.

A trial with $k \geq 2$ directional changes is defined as a wiggle (**Figure 2c–f**). We considered three possible interpretations of wiggles: (1) active sensing, (2) change-of-mind, and (3) disengagement.

- **Active sensing hypothesis:** Mice wiggle the wheel to enhance perception because it is easier to detect a moving visual stimulus than a static one. In this view, the jitter serves as a strategy for accumulating sensory evidence by dynamically modulating the visual input.
- **Change-of-mind hypothesis:** Mice wiggle the wheel due to uncertainty about the correct decision. In this view, the jitter represents hesitation between the leftward and rightward choices as the mouse re-evaluates its initial decision.
- **Disengagement hypothesis:** Mice wiggle the wheel because they are disengaged from the task. In this view, the jitter represents idle movements that are not goal-directed.

To address these alternative interpretations, we stratified wiggle trials by movement duration. We observed that a subset of trials involved prolonged wiggling (duration > 1 second) and long reaction times (> 1.2 seconds), consistent with behavioral disengagement. These trials comprised 6.7% of the data and had a mean number of direction changes of $k = 8.68$.

To exclude disengaged behavior, we restricted all subsequent analyses to wiggle trials with a duration up to 1 second. Within this restricted dataset, we aimed to distinguish between the active sensing and change-of-mind hypotheses.

	Active sensing	Change-of-mind
Trial history dependence	Weak	Strong (wiggle trials more frequent after errors)
Block congruency dependence	Weak	Strong (wiggle trials more frequent in block-incongruent condition)

Table 2: We hypothesized that wiggle trials explained by active sensing were not significantly dependent on trial history and block congruency.

We fit a binomial generalized linear model to $1,169,323$ trials from 213 mice with predictors for trial history dependence (β_1), block congruency (β_2), visual stimulus contrast (β_3), and their interaction (β_4) (see Methods 4.2.8). The dependent variable was the occurrence of wiggles. Each coefficient β represents a log-odds ratio.

We found that wiggles were less likely at higher contrast trials ($\beta_3 = -0.236, p < 0.001$). To interpret $\beta_3 = -0.236$, we computed $e^{-0.236} \approx 0.79$. This means that with each unit increase in absolute contrast, the odds of a wiggle multiples by 0.79 (a 21% decrease). This is consistent with the active sensing hypothesis, which posits that wiggles are more likely at lower contrast trials.

We also found that wiggles were more frequent following correct responses ($\beta_1 = 0.054, p < 0.001$). This trial history effect suggests that positive reinforcement may promote wiggling behavior. The main effect of block congruency was weak and only marginally significant ($\beta_2 = 0.052, p = 0.055$), and its interaction with previous trial outcome was not significant ($\beta_4 = 0.019, p = 0.063$). The distribution of k does not change for block congruent versus block incongruent stimuli (Wilcoxon signed-rank test; $W = 30.0, p = 0.76, N = 213$ mice). Together, these findings indicate that both visual uncertainty and recent trial history shape wiggling behavior, consistent with a form of active sensing modulated by internal state.

Wiggle trials were relatively uncommon and the proportion of trials decreases as k increases: (1) 60.1% in $k = 0$, (2) 18.1% in $k = 1$, (3) 12.4% in $k = 2$, (4) 4.8% in $k = 3$, and (5) 4.6% in $k \geq 4$. (**Figure 2f**). To achieve adequate statistical power, we pooled wheel movements with at least 4 directional changes into one group. We plotted k between 0 and 8 directional changes, which represents all of the data.

During low visual stimulus contrast trials, we observed wiggles with a multi-part wheel movement: (1) jitter that was often followed by (2) a ballistic movement. We hypothesized that mice sampled visual stimulus information with jitter and then swiped to the center with a ballistic movement when enough evidence was accumulated. We named this the "sample-then-swipe" strategy.

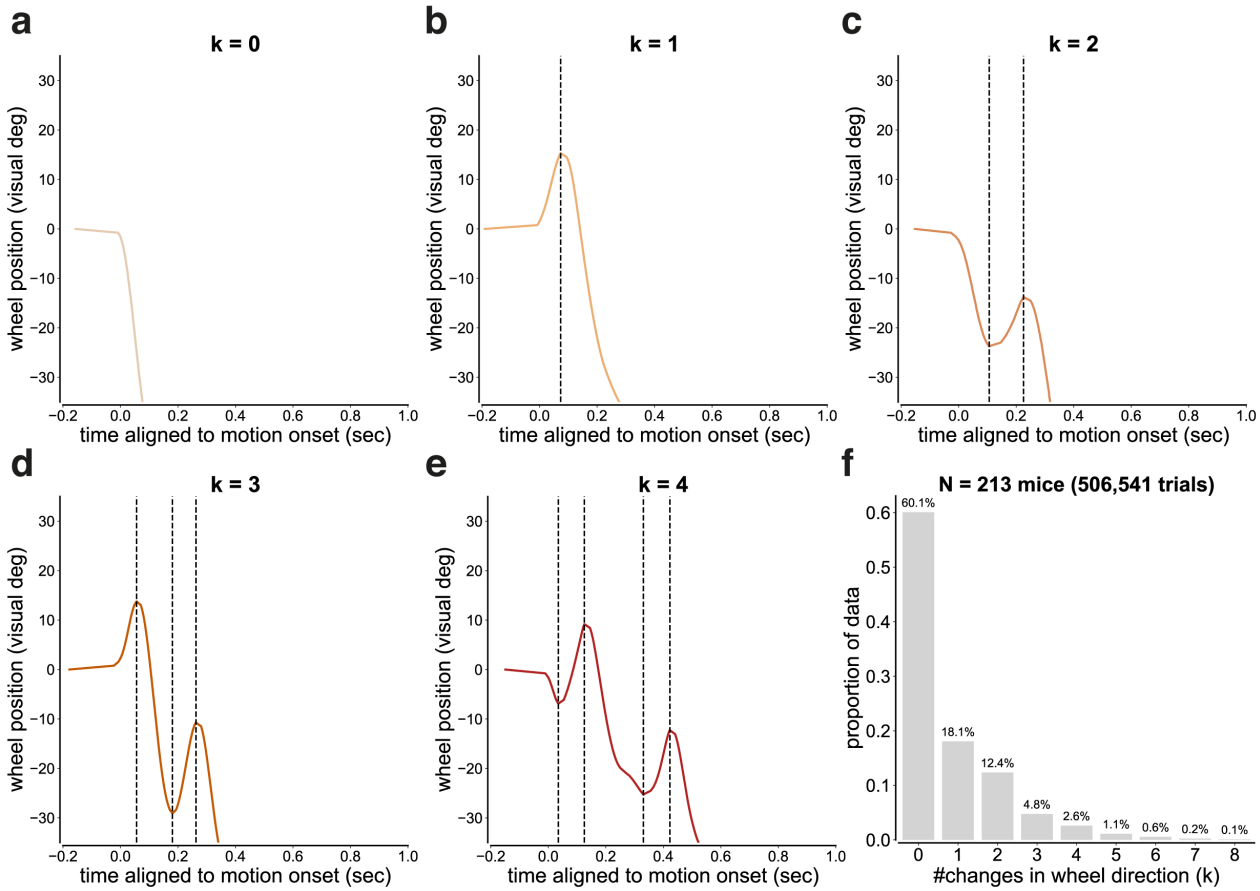

Figure 2: **Wiggles are wheel movements with multiple changes in wheel direction.** We computed the number of wheel directional changes (k) in each low visual stimulus contrast trial (0.0625 contrast). Single-trial examples of wheel data (position versus time) are shown are shown for **(a)** $k = 0$, **(b)** $k = 1$, **(c)** $k = 2$, **(d)** $k = 3$, and **(e)** $k = 4$ directional changes. Each trial is aligned to motion onset, which is defined as the time when the wheel velocity exceeded the threshold of 0.5 radians/sec after a minimum of 0.05 seconds of quiesence. **(f)** The distribution of k from $506,541$ low visual stimulus contrast trials in 213 mice is shown.

2.2 As the number of changes in wheel direction increases, the low visual stimulus contrast accuracy across mice increases.

To see if the low visual stimulus contrast accuracy changes with wiggles, we examined the relationship between wiggles and the proportion correct as a function of visual stimulus contrast. We expected that wiggles would be most effective when visual stimulus information was limited.

In behavioral data where the total time to choice was at most 1 second, we show that there is a positive correlation between the number of changes in wheel direction (k) and the low visual stimulus contrast accuracy (Pearson correlation, $r = 0.900, p = 0.038, N = 5$ group means computed from 213 mice) (**Figure 3a**). This effect remained statistically significant when we weighted each data point by the number of trials per session ($p = 0.038$), mitigating the influence of sessions with very few trials. A subset of such sessions that had 100% accuracy at $k \geq 4$ were based on as few as 1–2 trials. On average, we found that these sessions had only 3.06 trials (SD = 2.87), which suggests that sampling variability contributes to ceiling effects at high k values.

This was not seen in zero visual stimulus contrast trials, where the proportion correct was independent of k (Pearson correlation, $r = -0.087, p = 0.890, N = 5$ group means computed from 213 mice) (**Figure 3b**). Since zero visual stimulus contrast trials were rewarded based on the biased blocks (80/20 or 20/80), the proportion correct is greater than 50% ($0.8 \times 0.8 = 0.64$).

To demonstrate that wiggles are an active sensing strategy, we computed the wiggle occurrence independent of proportion correct as a function of visual contrast. Wiggle occurrence is defined as the proportion of wheel movements with at least 2 directional changes ($k \geq 2$). We expected that wiggles were most frequent during zero visual stimulus contrast and least frequent during high visual stimulus contrast. We show that the wiggle occurrence decreases as visual stimulus contrast increases (Pearson correlation, $r = -0.926, p = 0.024, N = 5$ group means computed from 213 mice), which is indicative of active sensing (**Figure 3c**). The wiggle occurrence decreases from $18.0 \pm 10.7\%$ (0.0 contrast) to $12.2 \pm 7.9\%$ (1.0 contrast).

The wiggle occurrence is non-zero during high visual stimulus contrast trials ($12.2 \pm 7.9\%$). This observation runs counter to the active sensing hypothesis, which posits that mice wiggle the wheel when visual information is limited. We hypothesized instead that mice may wiggle the wheel more when aroused, especially in high contrast conditions where decision certainty is minimal.

To address arousal as a potential confound in interpreting wiggle trials, we computed the wiggle duration as a function of visual contrast. Wiggle duration is defined as the total time spent in rapid, low-amplitude, back-and-forth wheel movements during a trial. This metric excludes periods of stillness or slow drift. We reasoned that if wiggles during low visual stimulus contrast reflect active sensing, they should be sustained for longer durations, whereas brief wiggles during high visual stimulus contrast would be more consistent with arousal-related jitter. We show that the wiggle duration decreases as visual stimulus contrast increases (Pearson correlation, $r = -0.984, p = 0.002, N = 5$ group means computed from 213 mice) (**Figure 3d**). Wiggle duration decreases from 0.47 ± 0.13 seconds (0.0 contrast) to 0.16 ± 0.10 seconds (1.0 contrast). This suggests that low visual stimulus contrast wiggles cannot be explained by arousal alone.

Next, we computed the wiggle amplitude as a function of visual contrast. This addresses the alternative hypothesis that mice are fidgeting with the wheel while wiggling. We expected that wiggles due to active sensing were high-amplitude wheel movements. During low visual stimulus contrast trials, we show that mice wiggle the wheel for 8.3 ± 2.5 visual degrees, which is about one-fifth of a complete trial (8/35 is 22%). The wiggle amplitude is not significantly dependent on visual stimulus contrast (Pearson correlation, $r = 0.855, p = 0.065, N = 5$ group means computed from 213 mice) (**Figure 3e**). Since wiggle duration but not wiggle amplitude is a function of visual contrast, this suggests that these movements are goal-directed rather than habitual.

In addition, we separated the wheel data by blocks. We expected that the relationship between low visual stimulus contrast accuracy and wiggles would be most positive during unbiased blocks, when choice is driven by visual stimulus information in the absence of block information. We show that accuracy improvement is 4% greater in unbiased blocks than biased blocks, which suggests that wiggles are more helpful in a visual detection task (**Figure 3f–g**).

Last, we compared decision accuracy between wiggle trials (≥ 4 directional changes) and non-wiggle trials (0 directional changes). Out of 201 mice, 86 showed significantly higher accuracy in wiggle trials and 115 showed significantly lower accuracy (Wilcoxon signed-rank test, $p < 0.05$) (**Figure 3h**). The distribution of wiggle-related changes was not consistent with random variation: mice that benefited had a median improvement of +8.3% (IQR: +4.3–19.3%), whereas non-benefiting mice showed a median decrease of −8.2% (IQR: −15.7 to −4.5%). Furthermore, 34% of all mice improved by more than +5%, indicating that the effect was substantial for a sizeable fraction of the population. Benefiting mice were less impulsive and exhibited fewer false starts than non-benefiting mice (**Figure S3**). Together, these results indicate that the relationship between wiggle trials and low visual stimulus contrast accuracy is heterogeneous across the mouse population.

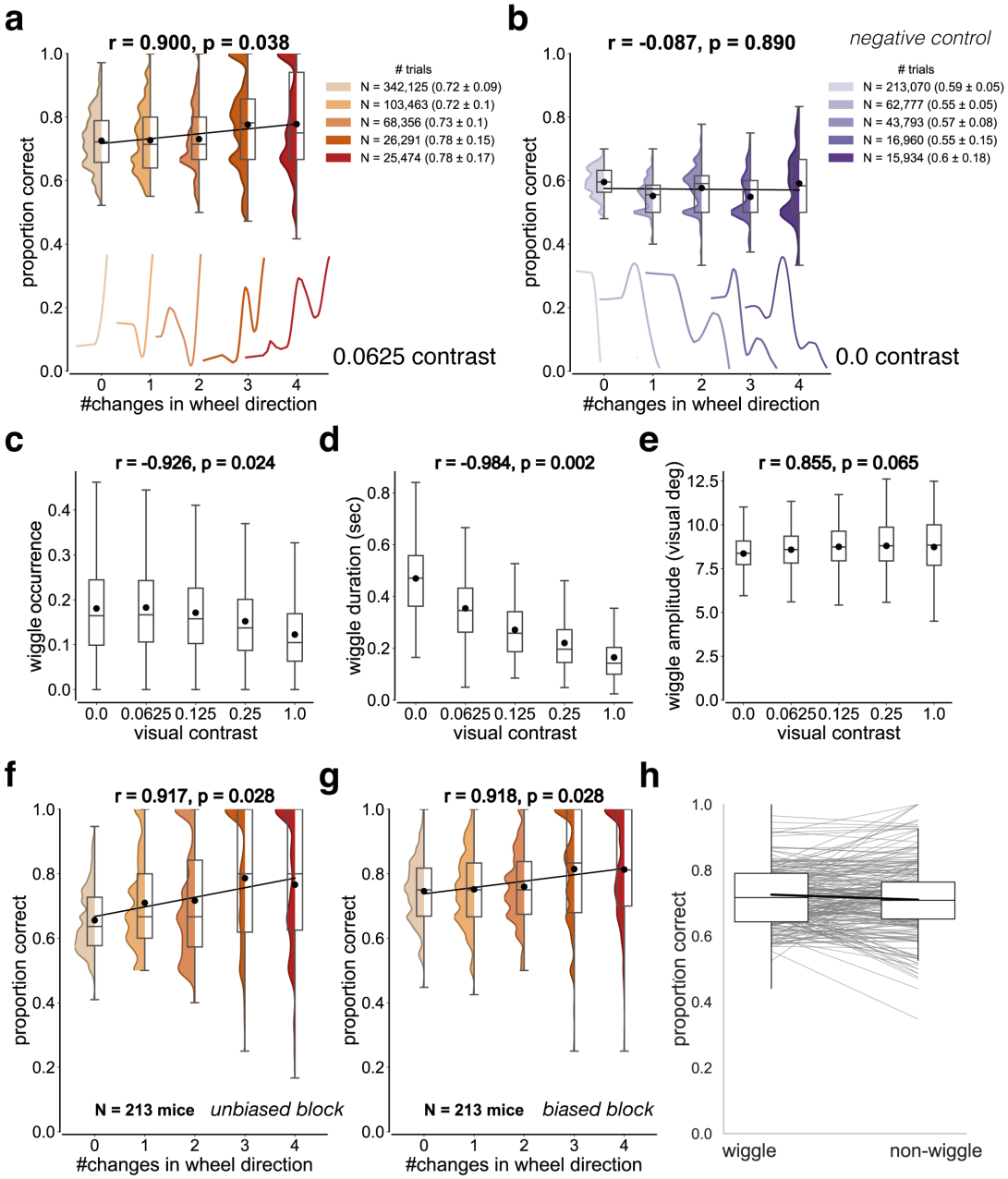

Figure 3: **As the number of changes in wheel direction increases, the low visual stimulus contrast accuracy across mice increases. (a - b)** The distributions of proportion correct across sessions as a function of visual stimulus contrast are shown. The legends report mean ± standard deviation. The mean of each group is represented as a black dot. Example wheel trajectories are shown for each k, which represents the number of changes in wheel direction. **(a)** The low visual stimulus contrast accuracy increases by 6.0% as k increases (Pearson correlation, $r = 0.900, p = 0.038, N = 5$ group means computed from 213 mice). **(b)** The zero visual stimulus contrast accuracy is independent of k (Pearson correlation, $r = -0.087, p = 0.890, N = 5$ group means computed from 213 mice). **(c - e)** We define wiggles as $k \geq 2$ movements. **(c)** The wiggle occurrence decreases as visual stimulus contrast increases (Pearson correlation, $r = -0.926, p = 0.024$, $N = 5$ group means computed from 213 mice). **(d)** The wiggle duration decreases as visual stimulus contrast increases (Pearson correlation, $r = -0.984, p = 0.002, N = 5$ group means computed from 213 mice). **(e)** The wiggle amplitude is independent of visual stimulus contrast (Pearson correlation, $r = 0.855, p = 0.065, N = 5$ group means computed from 213 mice). **(f - g)** The accuracy improvement for low visual stimulus contrast associated with wheel directional changes is 4% greater in unbiased blocks (50/50: 10% improvement) than biased blocks (20/80 or 80/20: 6% improvement). **(h)** Accuracy comparison between wiggle trials (≥4 directional changes) and non-wiggle trials (0 directional changes) at 0.0625 contrast. Each gray line connects the two conditions for one mouse (≥10 trials per type), black points are subject means scaled by trial count, and the thick black line is the trial-count–weighted mean across subjects. Across 201 mice, 86 showed significantly higher accuracy in wiggle trials and 115 showed significantly lower accuracy (Wilcoxon signed-rank test, $p < 0.05$). Benefiting mice improved by a median of +8.3% (IQR: +4.3% to +19.3%), whereas non-benefiting mice showed a median decrease of −8.2% (IQR: −15.7% to −4.5%). Overall, 34% of mice improved by more than +5% during wiggle trials.

2.3 Mice wiggle the wheel at speeds that generate visual temporal frequencies close to the range of maximal contrast sensitivity during low visual stimulus contrast trials.

To connect the wheel movement to visual stimulus movement, we first converted wheel speed (in wheel degrees per second) to visual stimulus speed (in visual degrees per second). The conversion factor was 1 wheel degree is about 2 visual degrees. We then divided the visual speed by the spatial frequency of the Gabor patch (0.1 cycles per degree) to obtain the effective temporal frequency experienced by the mouse. This temporal frequency reflects how rapidly the stimulus pattern drifted across the retina as the mouse wiggled the wheel.

We next examined whether low visual stimulus contrast accuracy depended on the temporal frequency generated by wiggles. Specifically, we quantified the relationship between temporal frequency and proportion correct as a function of the number of changes in wheel direction. Based on contrast sensitivity functions, we expected wiggles to be most effective when they produced temporal frequencies near the range of maximal sensitivity.

We first show that the number of changes in wheel direction (k) is negatively correlated with the temporal frequency of the visual stimulus (Pearson correlation, $r = -0.871, p = 0.129, N = 4$ group means generated from 213 mice) (**Figure 4a**). Temporal frequency is highest during $k = 1$ movements (18.78 ± 3.05 Hz) and lowest during $k \geq 4$ movements (11.52 ± 2.45 Hz). We hypothesized that this negative correlation reflects a constraint imposed by mouse temporal contrast sensitivity: $k = 1$ movements may produce visual motion that is too fast to be perceptible by mice, whereas $k \geq 4$ movements may produce visual stimulus modulations that are within the range of mouse visual acuity.

To test this, we asked whether mice wiggle the wheel at a temporal frequency that aligns with the peak contrast sensitivity of the mouse visual system. We compared our behavioral data to the only published temporal contrast sensitivity (TCS) curve for mice (Umino et al, 2018). We found that the average temporal frequency during $k \geq 4$ wiggles (11.52 ± 2.45 Hz) closely matches the frequency at which mouse TCS peaks (12 Hz; TCS = 2.69, SEM = 0.36; **Figure 4b**). Although $k \geq 4$ wiggles represent a small proportion of the data (13.7%; **Figure 2f**), the overall dataset is large (25,474 trials from 213 mice), which provides sufficient power to estimate the average temporal frequency. Based on a one-sample t-test, the observed difference from the reference value (12 Hz) corresponds to a small effect size (Cohen's d = 0.196), with an estimated power of 81.2% at $\alpha = 0.05$. Taken together, these findings suggest that mice are able to perceive the left-to-right visual motion elicited by wiggle movements.

It is important to note that the TCS data is based on full-field visual stimulus whereas the wheel data is based on a local visual stimulus. In the study by Umino and colleagues, the TCS is equal to the sensitivity index of freely moving mice during a Go/No-Go task that manipulated temporal frequency at about the same spatial frequency (see Methods 4.2.10).

We also observed that the wiggle temporal frequency data is variable. For example, the standard deviation in $k \geq 4$ directional changes is large (2.45 Hz is about 20% of 11.52 Hz). This illustrates that wiggles are not periodic but vary in amplitude and duration within and across trials.

Next, we asked if higher visual temporal frequencies generated by mouse wiggles were more accurate for a given number of changes in wheel direction. We binned temporal frequency data for a fixed k and computed the low visual stimulus contrast accuracy across bins. For $k = 2$ trials, the correlation was weak and non-significant (Pearson correlation, $r = 0.299, p = 0.472, N = 8$ group means generated from 213 mice; **Figure 4c**), while stronger and statistically significant correlations emerged for $k = 3$ trials (Pearson correlation, $r = 0.737, p = 0.037, N = 8$ group means generated from 213 mice; **Figure 4d**) and $k \geq 4$ trials (Pearson correlation, $r = 0.771, p = 0.025, N = 8$ group means generated from 213 mice; **Figure 4e**).

The within-k analysis in **Figures 4c–e** is consistent with the across-k analysis in **Figure 4b** up to 12 Hz. **Figure 4b** shows that the median temporal frequencies in $k = 2$, $k = 3$, and $k \geq 4$ trials are close to the peak mouse TCS. In line with this, **Figures 4c–e** show that the proportion correct is above chance level up to 12 Hz.

However, an inconsistency emerges in the following temporal frequency bins: 15 Hz, 18 Hz, and 21 Hz. While **Figure 4b** predicts that proportion correct decreases at temporal frequencies above 12 Hz, **Figures 4c–e** do not show a drop in accuracy. We believe this inconsistency emerges because of a drop in data in those bins. For instance, there are 14,470 trials at 12 Hz for $k \geq 4$, but only 8,735 trials at 15 Hz, 5,205 trials at 18 Hz, and 2,969 trials at 21 Hz. This reduction in data likely limits the statistical power to detect a decline in accuracy at high temporal frequencies, even if such a decline is present.

Last, we asked what proportion of mice show a positive relationship between temporal frequency and low visual stimulus contrast accuracy during $k \geq 4$ directional changes. We found that 46% of mice show significant positive correlations between temporal frequency and proportion correct during $k \geq 4$ directional changes, which is well above chance level (5% of mice) (**Figure 4f–g**). This suggests that individual mice benefit from high visual temporal frequencies of about 12 Hz generated by wheel movement.

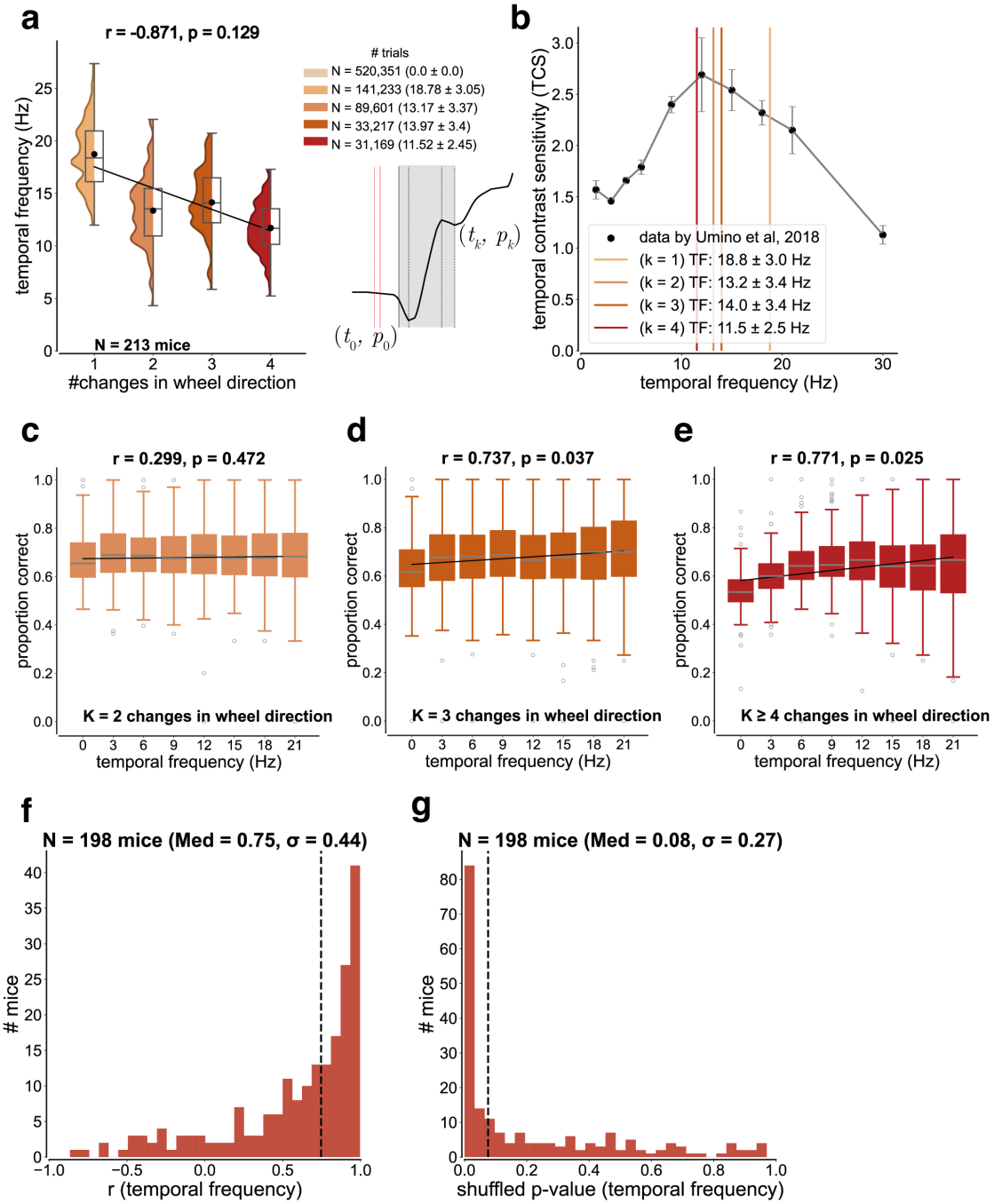

Figure 4: **Mice wiggle the wheel at speeds that generate visual temporal frequencies close to the range of maximal contrast sensitivity during low visual stimulus contrast trials. (a)** The distributions of temporal frequency across sessions during low visual stimulus contrast trials are shown. The legends report mean ± standard deviation. The mean of each group is represented as a black dot. The time window of analysis is indicated by the gray shaded region. There is a non-significant trend towards decreasing temporal frequency as wheel directional changes increase (Pearson correlation, $r = -0.871, p = 0.129, N = 4$ group means generated from 213 mice). **(b)** During $k \geq 4$ directional changes, mice wiggle the wheel at 11.5 ± 2.5 Hz, which is near the temporal frequency with maximum temporal contrast sensitivity (indicated by a red line at 12 Hz from data by Umino et al, 2018). Performance analysis shows that: **(c)** During $k = 2$ directional changes, the proportion correct is independent of temporal frequency (Pearson correlation, $r = 0.299, p = 0.472, N = 8$ group means generated from 213 mice). **(d)** During $k = 3$ directional changes, the proportion correct increases with temporal frequency (Pearson correlation, $r = 0.737, p = 0.037, N = 8$ group means generated from 213 mice). **(e)** This relationship is strongest in $k \geq 4$ directional changes (Pearson correlation, $r = 0.771, p = 0.025, N = 8$ group means generated from 213 mice). **(f)** The distribution of correlation coefficients (r) between temporal frequency and proportion correct in $k \geq 4$ directional changes within mice is negatively-skewed (skew $= -1.33, p = 4.15 \times 10^{-10}, N = 213$ mice). The median is indicated as a black dashed line. **(g)** The corresponding distribution of p-values based on a permutation test is shown ($n = 1000$ shuffles). There are 92 mice with $r > 0$ and $p < 0.05$, which indicates that 46% of mice show significant positive correlations between visual temporal frequency and proportion correct.

2.4 There are individual mice that benefit from wiggles during low visual stimulus contrast trials.

To address the modest effect sizes observed in our population-level analyses, we demonstrate clear examples of individual mice that benefit from wiggles during low visual stimulus contrast trials. Wiggles were quantified using three metrics of movement: motion energy, number of changes in wheel direction (k), and the visual temporal frequency.

Motion energy is distinct from visual temporal frequency, which is the wiggle speed divided by the stimulus spatial frequency. While motion energy captures the overall intensity of movement, wiggle speed quantifies how rapidly mice jitter the wheel back and forth. These metrics were treated differently in our analyses: the ballistic component of wiggle trials was excluded from the temporal frequency analysis (see Equation 3) but included in the motion energy analysis (see Equation 5).

In **Figure 5a**, we show a mouse (ibl_witten_16) that had a positive relationship between wiggles and accuracy at low contrast based on discrete (k) and continuous (motion energy and temporal frequency) metrics of wheel movement. Moreover, the accompanying heat map reveals that this mouse wiggled more frequently during low visual stimulus contrast trials and maintained this pattern consistently throughout the experiment.

In **Figure 5b**, we show another example mouse (ZFM-04300) that had the same positive relationship based on motion energy and k, but not temporal frequency. We believe this may be due to a drop-off in temporal frequency data generated by high-speed wiggles. While the heat map of this mouse is less systematic and there are wiggles in the higher visual stimulus contrast trials, the predominant pattern still shows increased wiggling frequency during low visual stimulus contrast trials, sustained across experimental sessions.

These individual examples illustrate that despite modest population-level effects, specific mice demonstrate clear and consistent benefits from wiggle behavior, supporting the biological relevance of this phenomenon.

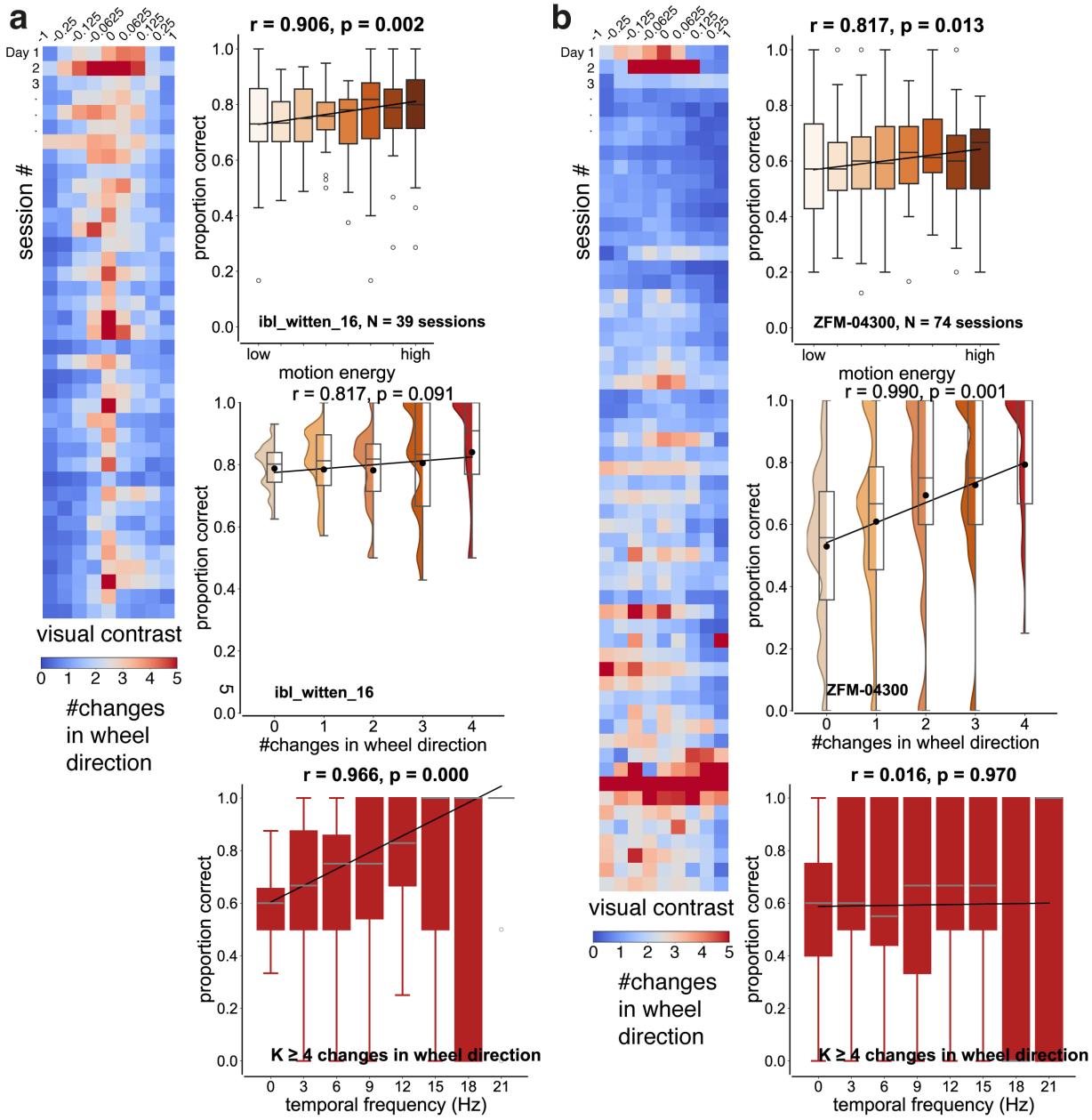

Figure 5: **There are individual mice that benefit from wiggles during low visual stimulus contrast trials. (a) ibl_witten_16:** This mouse shows a positive relationship between wiggles and accuracy at low visual stimulus contrast, as measured by motion energy (Pearson correlation, $r = 0.906, p = 0.002, N = 8$ group means from 39 sessions), number of changes in wheel direction (k) (Pearson correlation, $r = 0.817, p = 0.091, N = 5$ group means from 39 sessions), and visual temporal frequency (Pearson correlation, $r = 0.966, p < 0.001, N = 8$ group means from 39 sessions). **(b) ZFM-04300:** This mouse also shows a positive relationship based on motion energy (Pearson correlation, $r = 0.817, p = 0.013, N = 8$ group means from 74 sessions) and k (Pearson correlation, $r = 0.990, p = 0.001, N = 5$ group means from 74 sessions), but not visual temporal frequency (Pearson correlation, $r = 0.016, p = 0.970, N = 8$ group means from 74 sessions). **(a - b)** Heat maps show k versus visual stimulus contrast across experimental sessions.

2.5 As the motion energy increases, the low visual stimulus contrast accuracy across mice is constant.

To test whether movement intensity was correlated with accuracy, we examined the relationship between motion energy and proportion correct as a function of visual stimulus contrast. We expected that higher motion energy wiggles would be more effective, since larger wheel displacements would generate bigger visual stimulus movements.

However, low visual stimulus contrast accuracy did not vary systematically with motion energy (Pearson correlation, $r = 0.0048, p = 0.632, N = 8$ group means computed from 213 mice) (**Figure 6a**). A corresponding negative control is shown for zero visual stimulus contrast trials (**Figure 6b**). Together, these results suggest that population-level analyses may obscure the role of motion energy, as the mouse population is heterogeneous and the task was not explicitly designed with wiggles in mind.

To further address the null hypothesis that wiggles are irrelevant for performance, we next quantified the proportion of individual mice that showed performance benefits from wiggling based on motion energy.

Across $N = 209$ mice, we identified 20 such mice with a significant positive correlation between motion energy and low visual stimulus contrast accuracy, which is 10% of the population (**Figure 5c–d**). This result is based on a permutation test, where we shuffled accuracy values relative to motion energy within each mouse 1000 times to build a null distribution of the number of "significant positives" expected by chance. Under the null hypothesis, we would expect 5% of the population (≈10 mice) to show significant positive correlations by chance alone. The observed number of mice with significant positive correlations is approximately twice the expected false-positive count, suggesting that a subset of mice benefit from wiggling when visual information is limited.

Among these 20 mice, the mean correlation coefficient was $r = 0.77$ (IQR: $0.69 - 0.86$), indicating a substantial behavioral effect size in this subgroup. These findings support the hypothesis that wiggling movements can enhance low visual stimulus contrast accuracy by increasing stimulus salience through self-generated motion in a subset of mice.

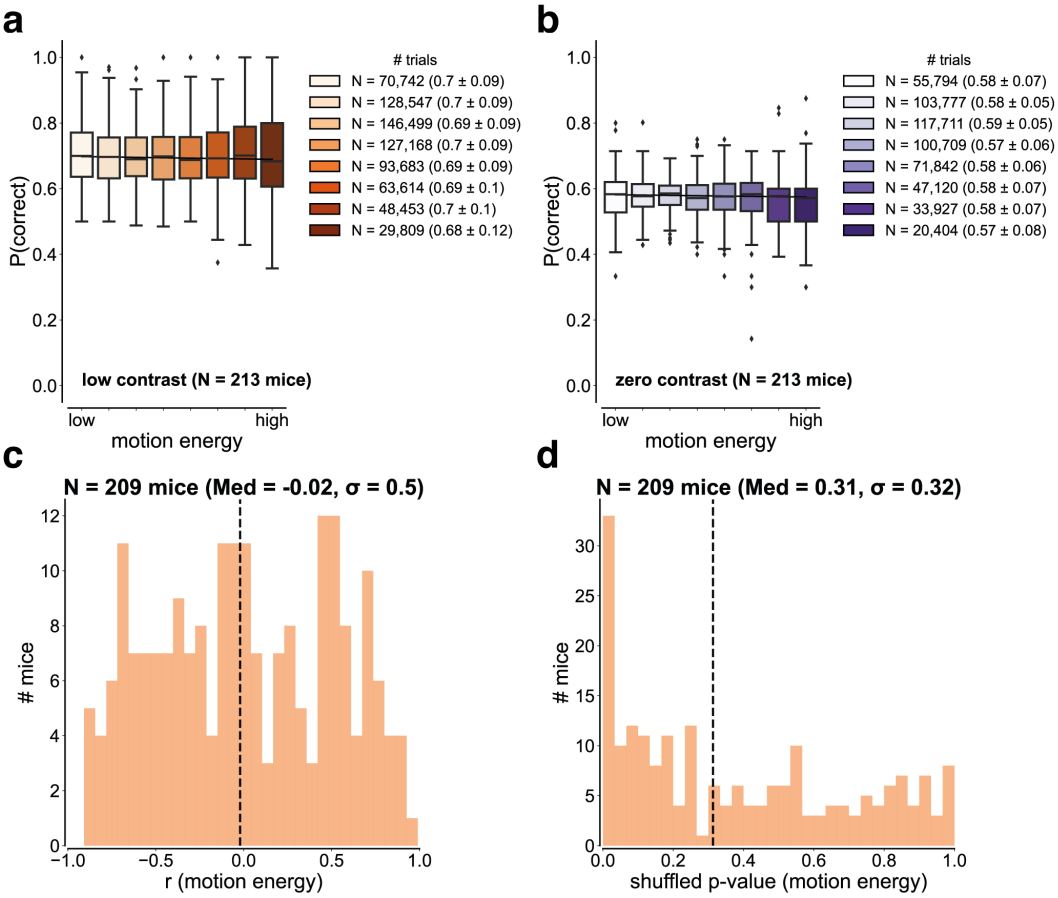

Figure 6: **As the motion energy increases, the low visual stimulus contrast accuracy across mice is constant.** **(a)** The low visual stimulus contrast accuracy is not significantly dependent on motion energy (Pearson correlation, $r = 0.0048, p = 0.632, N = 8$ group means computed from 213 mice). **(b)** A corresponding negative control is shown for zero visual stimulus contrast trials. **(c)** Population-level analysis shows the distribution of correlation coefficients between motion energy and proportion correct during low visual stimulus contrast trials is not significantly skewed (skew $= 0.15$, $p = 0.878, N = 209$ mice). The median is indicated as a black dashed line. **(d)** The corresponding distribution of p-values from permutation tests ($n = 1000$ shuffles) shows 20 mice with significant positive correlations ($r > 0$ and $p < 0.05$), representing 10% of the population.

2.6 Wiggle duration enhances stimulus side decoding accuracy in midbrain and thalamic regions.

To test if wiggles improve the detection of low visual contrast stimuli in neural data, we applied a logistic regression decoder analysis to single-trial, single-neuron electrophysiology data (The International Brain Laboratory, 2023). We hypothesized that stimulus side decoding would be more accurate during wiggle trials than non-wiggle trials. However, the input to a decoder needs to be the same length from both conditions, and a non-wiggle is much faster than a wiggle (movement duration of about 0.2 seconds versus 1 second). The ideal control is with long, non-wiggling durations that do not come from losing focus, motivation, or attention. The caveat is that such trials do not exist.

We instead asked if stimulus side decoding accuracy improves over the duration of a wiggle. We compared decoding accuracy between short (0.2 seconds) and long (1 second) wiggle durations across multiple brain areas.

We show that this is indeed the case in midbrain and thalamic regions. In the midbrain, both the superior colliculus (SC) and anterior pretectal nucleus (APN) showed significant improvements in decoding accuracy with longer wiggles (SC: $p < 0.001$, +3% accuracy; APN: $p < 0.001$, +5% accuracy; **Figure 7a**). Similarly, the lateral posterior nucleus of the thalamus (LP) exhibited a significant decoding enhancement ($p = 0.001$, +3% accuracy; **Figure 7b**). Positive control analyses in the primary motor cortex (MOp) confirmed expected improvements ($p = 0.001$, +2% accuracy; **Figure 7c**), whereas the negative control in auditory cortex (AUD) showed no significant change ($p = 0.124$, +1% accuracy; **Figure 7d**). These results demonstrate that extended wiggle duration selectively improves neural representations of stimulus side in subcortical regions, which is consistent with the hypothesis that longer wiggles provide more visual stimulus information than shorter wiggles.

It is important to note that decoding accuracy did not improve with longer wiggles in the primary visual cortex (V1: $p = 0.382$, -0.7% accuracy) but it did in the antero-medial primary visual area (VISa: $p = 0.035$, +2.2% accuracy) (**Figure S5**). This aligns with an analysis of the proportion of neurons with increased firing during wiggles compared to non-wiggles 400 msec after stimulus onset (VISa: 16.67%, SC: 10.93%, V1: 8.37%) in 0.0625, 0.125, and 0.25 visual stimulus contrast trials (**Figure 8a**). This distribution changes in 0.0 visual stimulus contrast trials (VISa: 6.25%, SC: 18.01%, V1: 7.11%) in the absence of visual feedback (**Figure 8c**), which suggests that wiggle-related modulation in visual areas does not reflect an efference copy. Taken together, these results indicate that wiggling can be detected in the neural data.

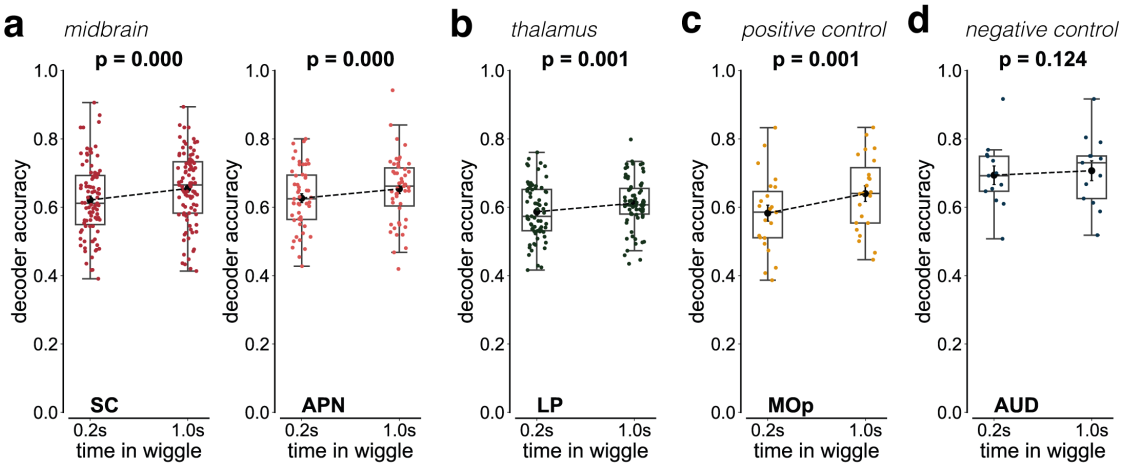

Figure 7: **Wiggle duration enhances stimulus side decoding accuracy in midbrain and thalamic regions. (a - d)** We trained a logistic regression decoder to predict stimulus side (left or right) from neural activity in a given brain region as a function of wiggle duration (0.2 seconds versus 1 second). Single trial, single-neuron post-stimulus onset activity was used as an input (see Methods 4.1.2 and 4.2.9), including only trials with a visual stimulus contrast between 0% and 100%. Sessions with fewer than 20 wiggle trials were excluded. Neural data was binned in 20 ms windows, and decoding was repeated 100 times with stratified train-test splits. Brain region abbreviations and colors follow the Allen Institute Brain Atlas (SC: superior colliculus; APN: anterior pretectal nucleus; LP: lateral posterior nucleus of the thalamus; MOp: primary motor cortex; AUD: auditory cortex). All comparisons used a Wilcoxon signed-rank test ($\alpha = 0.05$). **(a)** Midbrain regions show significant improvements: SC ($p < 0.001, N = 91$ sessions, 3% improvement) and APN ($p < 0.001, N = 51$ sessions, 5% improvement). **(b)** Thalamic LP also shows significant improvement ($p = 0.001, N = 72$ sessions, 3% improvement). Controls confirm the specificity: **(c)** positive control MOp shows expected significant improvement ($p = 0.001, N = 23$ sessions, 2% improvement) while **(d)** negative control AUD shows no significant change ($p = 0.382, N = 25$ sessions, 1% improvement).

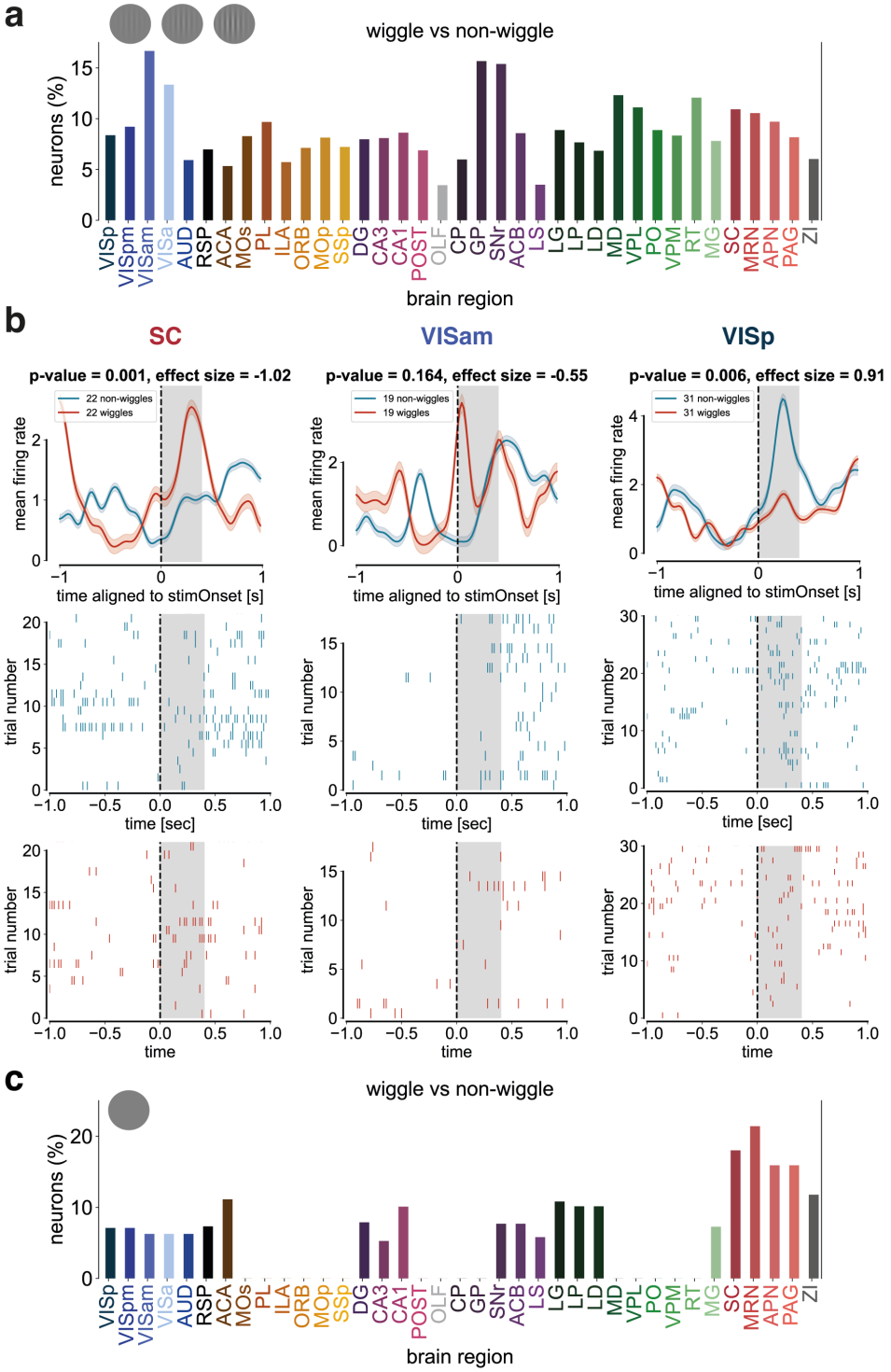

Figure 8: **Proportion of neurons with increased firing during wiggles versus non-wiggles 400 ms after visual stimulus onset. (a)** Across $N = 37$ brain regions, the fraction of neurons (%) with a significantly higher normalized mean firing rate during wiggles compared to non-wiggles is shown. Significance was defined as $p \leq 0.05$ (Wilcoxon signed-rank test) and Cohen's $d \geq 0.8$. Spikes were counted in 20 ms bins, smoothed with a Gaussian kernel ($\sigma = 3$ bins), and normalized by dividing by baseline firing rate (–0.5 to 0 s relative to stimulus onset) + 1 spike/s. To have enough wiggle trials for analysis, the 0.0625, 0.125, and 0.25 visual stimulus contrast trials were used. For each wiggle trial, the closest non-wiggle trial in session time was used for comparison. The highest proportion of neurons was observed in the antero-medial primary visual area (VISam: 16.67%), and the lowest in the olfactory area (OLF: 3.45%). Brain region abbreviations and colors follow the Allen Institute Brain Atlas. **(b)** Corresponding single-cell example responses aligned to visual stimulus onset are shown for the superior colliculus (SC), antero-medial primary visual area (VISam), and primary visual cortex (VISp). **(c)** Corresponding negative control in zero visual stimulus contrast trials is shown.

3 Discussion

Our first claim is that mouse wheel wiggling is an example of active sensing. There is a significant positive relationship between low visual stimulus contrast accuracy and the number of changes in wheel direction across 213 mice, and the regression line is statistically significantly different from zero ($p = 0.038$) (**Figure 3a**). This effect is not as strong as expected because it includes 110 mice with a monotically increasing correlation, 24 mice with a monotically decreasing correlation, and 69 mice with a non-monotonically increasing correlation (**Figure S1**). This effect is also weakened by biased blocks, which diminish the role of visual stimulus information and likely result in fewer wiggle trials. Despite the heterogeneity of the mouse population and relative uncommoness of wiggle trials, we were still able to demonstrate a substantial positive correlation across mice. These effects were even more obvious within mice that benefit from an active sensing strategy (**Figure 5**).

Our second claim is that mice wiggle the wheel at a natural temporal frequency for the visual system. Active sensing movements are often rapid compared to the speed of sensory transduction itself (Born, 2009). Mice wiggle the wheel at 11.52 ± 2.45 Hz during $k \geq 4$ directional changes (**Figure 3a**), which is much higher than the $1-2$ Hz preferred temporal frequency of mouse V1 neurons (Marshel et al, 2011; Han et al, 2022). However, the temporal frequency at which mice wiggle the wheel aligns well with the maximum temporal contrast sensitivity identified by Umino and colleagues in a Go/No-Go task, which was 12 Hz (**Figure 4b**). This finding should be interpreted in light of the limitations outlined in **Table 2**, where the greatest caveat is the difference between full-field versus localized visual stimulus. We believe that these discrete, rapid, and repetitive wheel movements create large changes in sensory signals.

Our third claim is that the proportion of mice that benefit from wiggling during low visual stimulus contrast trials is above chance level. We identified 92 mice with a significant positive correlation between temporal frequency and accuracy, representing 46% of the mouse population (**Figure 4f–g**). By contrast, a motion energy analysis revealed only 20 mice (10%) with a significant positive correlation (**Figure 5e–f**). Both analyses indicate that the proportion of mice benefiting from wiggling is greater than that expected by chance (5% or 10 mice), but they diverge in the strength of the observed effects.

We believe that this divergence can be explained by using the entire wheel trajectory in motion energy analysis but using only the wheel jitter in temporal frequency analysis. Brief, high-speed movements and prolonged, low-speed movements can yield similar motion energies, making speed a more sensitive measure of the active sensing benefit. As a result, our strongest effects were captured in a speed-based analysis that was converted to temporal frequency units.

Experimental factors likely contributed to the modest effect sizes observed in population-level analyses. First, most of the behavioral data was acquired during biased blocks. Since mice could exploit the block structure of the task rather than relying solely on the visual stimulus for decisions, this reduced their dependence on wiggles for perceptual enhancement. Second, the spatial frequency of the visual stimulus was above the perceptible threshold. This meant that mice could perceive low visual contrast stimuli without wiggles. Redesigning the task to present more difficult visual stimuli at the perceptual threshold would likely reveal substantially larger benefits from wiggles. Third, the heterogeneous nature of wiggle responses across individual mice means that population averages obscure both the mice that benefit from wiggles and those that do not, diluting the overall effect size and masking the biological significance of this behavior.

Our work highlights the role of "watching and wondering" about behavior in large-scale data analysis (Tinbergen, 1973). Data analysis within and across mice revealed a substantial positive relationship between wiggles and low visual stimulus contrast accuracy. The large number of trials and animals in our dataset also lends confidence to the robustness of the effect. We believe that mice wiggle the wheel to boost the salience of low visual contrast stimuli.

3.1 Potential underlying neuronal circuit

One reason that wiggles are an effective strategy for mice performing this perceptual decision-making task is that the visual stimulus is always oriented vertically. This means that when a mouse jitters the wheel left-to-right, it switches between black and white stripes as the low-contrast Gabor patch moves horizontally on the screen. A study by Millman and colleagues found that vasoactive intestinal peptide (VIP) interneurons in mouse V1 were sensitive to low-contrast nasal-to-temporal motion on the retina (Millman et al, 2020). Although this differs from how mouse wiggles move the visual stimulus (left-to-right versus front-to-back), it suggests that VIP interneurons contribute to processing low-contrast retinal motion.

For cortical neurons in the retinotopic location of the visual stimulus, a moving visual stimulus would move from one neuron's receptive field to a second neuron's receptive field. This means that two neurons are excited at different times by the dynamic visual stimulus. Thus, a neural circuit mechanism of mouse wiggles likely involves sequentially activating neurons with retinotopically-aligned receptive fields to the visual stimulus.

4 Methods

4.1 Experimental model and subject details

All procedures and experiments were carried out in accordance with the local laws and following approval by the relevant institutions: the Animal Welfare Ethical Review Body at University College London; the Institutional Animal Care and Use Committees of Cold Spring Harbor Laboratory, Princeton University, University of Washington, University of California at Berkeley and University of California at Los Angeles; the University Animal Welfare Committee of New York University; and the Portuguese Veterinary General Board.

4.1.1 Mice

A total of 213 adult mice (C57BL6/J, 163 male, 50 female, age: 29.92 ± 13.47 weeks) were used for analysis. Mice were kept in a 12-hour light-dark cycle and performed the task in the dark period (from 7:00 to 19:00). Details are available here: (Appendix 1 of The International Brain Laboratory, 2021).

4.1.2 Electrophysiological data

Spike counts were obtained by summing spikes across time for both wiggle and non-wiggle trials. The neural data matrix had dimensions $N \times T \times K$, corresponding to N neurons, T time bins, and K trials, with indices $n = 1, \ldots, N$ and $t = 1, \ldots, T$. The bin size was 0.02 seconds. The input to the logistic regression decoder was the single-trial neural activity, given by:

$$X \in \mathbb{R}^{K \times (N \times T)} \tag{1}$$

Each input vector to the logistic regression decoder is a flattened neural population activity per trial reshaped to a row vector of length $N \cdot T$:

$$x^{(i)} \in \mathbb{R}^{(N \times T)}, i = 1, \ldots, K$$

	time window aligned to stimulus onset
post-stimulus decoder	$[0, 0.2]$ and $[0, 1]$

Table 3: We performed decoder analysis in the time windows above.

4.2 Quantitative and statistical analysis

4.2.1 Inclusion criteria for analysis

Trial Trials with a a duration less than or equal to 1 second and a go-cue onset and visual stimulus onset within 0.05 seconds were included in this analysis.

Session Sessions with a minimum of 1 trial in each group were included in this analysis unless otherwise stated. There were 5 groups based on number of changes in wheel direction: (1) $k = 0$, (2) $k = 1$, (3) $k = 2$, (4) $k = 3$, and (5) $k \geq 4$.

Insertion Electrode insertions with a maximum of 80 microns of drift and a minimum of 10 units were included in this analysis.

4.2.2 Psychometric curves

To obtain a psychometric curve, data points were fitted with the following parametric error function, using a maximum likelihood procedure:

$$P = \gamma + (1 - \gamma - \lambda) \frac{erf\left(\frac{c-\mu}{\sigma}\right)}{2} \tag{2}$$

P probability of rightward choice

c visual stimulus contrast (%)

γ lapse rate for left visual stimuli

λ lapse rate for right visual stimuli

μ	response bias
σ	contrast threshold

A detailed psychometric curve fitting procedure is in Protocol 2 (The International Brain Laboratory, 2020b).

The **lapse rate** (λ) is defined as the probability of an incorrect response independent of the visual stimulus contrast (Prins et al, 2012). It captures the difference between observed performance and perfect performance at the asymptotes (Gupta et al, 2024).

4.2.3 Definition of wiggles

Wiggles are defined as movements with greater than or equal to 2 changes in wheel direction from trial start (pre-quiescent duration) to end (feedback time). A change in wheel direction is defined as an extremum in the wheel position (deg) vs time (sec) data.

Note: An equivalent analysis was done such that a change in wheel direction is defined as a sign change in the wheel velocity (deg/sec) vs time (sec) data.

4.2.4 Definition of wiggle speed

Wiggle speed is defined as the total angular distance between each pair of extrema divided by duration in wheel position (deg) vs time (sec):

$$v = \begin{cases} \dfrac{1}{t_k - t_0} \displaystyle\sum_{i=0}^{k} |\theta_{i+1} - \theta_i| & k \neq 0 \\ \frac{|\theta_f - \theta_0|}{t_f - t_0} & k = 0 \end{cases} \tag{3}$$

k	total number of extrema
t_k	time of final extremum (sec)
t_0	time of motion onset (sec)
θ_k	position of extremum (deg)
θ_0	position of motion onset (deg)
t_f	time of feedback (sec)
θ_f	position of feedback (deg)

Note: To restrict wheel movement analysis to wiggles, the time period used for analysis was from the first inflection point (t_0) to the last extremum (t_k). The objective was to exclude the final ballistic movement in some trials, which would otherwise dominate the analysis.

4.2.5 Definition of visual angle

Visual angle is the perceived size of a stimulus given by:

$$\phi = 2 \arctan\left(\frac{h}{2d}\right) \tag{4}$$

h	height of monitor (cm)
d	distance between mouse and monitor (cm)
ϕ	visual angle (deg)

Mice viewed a Gabor patch on a screen size of 246 mm diagonal active display area and were positioned 8 cm away from the screen to achieve 102 visual degrees azimuth (The International Brain Laboratory, 2021). Based on Equation 4, the Gabor patch size is 19.7 cm if $\phi = 102^{\circ}$ and $d = 8$ cm.

Visual angle represents the size of an object's image on the retina. To obtain visual angle, we converted from wheel degrees to visual degrees. 35 visual degrees equals 17.2 wheel degrees (0.3 radians). Thus, 2 visual degrees corresponds to about 1 wheel degree.

4.2.6 Definition of motion energy

Motion energy is defined as the sum of squared speeds over each 0.05 second bin multiplied by the bin duration in wheel position (deg) vs time (sec):

$$\sum_{i=1}^{N} \left(\frac{\theta_{i+1} - \theta_i}{0.05} \right)^2 \cdot 0.05 \tag{5}$$

θ_i	position at start of i-th bin (deg)
θ_{i+1}	position at end of i-th bin (deg)
N	number of bins

4.2.7 Assessing statistical significance

Group-Level Analysis

A generalized linear mixed-effects model was used to compare non-wiggle with wiggle trials for the same mice in different laboratories. The median proportion correct for each group was obtained from each mouse. The pooled data was not weighted at this stage because the median value per mouse represented a weighted average by number of trials. Each mouse was treated as an independent sample.

Based on the negligible effect of inter-laboratory variance (0.002), a linear regression model was used to compare the number of wheel direction changes with low visual stimulus contrast accuracy for the same mice in different laboratories to obtain a p-value.

To compute the inter-laboratory variance, we used:

$$Y_{ij} = \beta_0 + \beta_1 Group_{ij} + \beta_2 Contrast_{ij} + \beta_3 Group_{ij} \cdot Contrast_{ij} + u_j + \epsilon_{ij} \tag{6}$$

Y_{ij}	proportion correct (dependent variable) for observation i in group j
β_0	intercept (the baseline proportion correct when contrast = low and group = 0)
β_1	coefficient for the effect of group (number of changes in wheel direction) on proportion correct
β_2	coefficient for the effect of contrast (high, low, or zero) on proportion correct
β_3	coefficient for the interaction effect between group and contrast
u_j	random effect for group j that represents inter-laboratory variance, which is assumed to be normally distributed with mean 0 and variance σ_u^2
ϵ_{ij}	residual error term for observation i in group j, representing unexplained variability, which is also assumed to be normally distributed with mean 0 and variance σ_ϵ^2

Each component represents:

1. **Intercept** (β_0): This term represents the expected proportion of correct movements when group = 0 and contrast = low. It represents a baseline performance for the average contrast and group.

2. **Group effect** ($\beta_1 Group_{ij}$): This term quantifies the change in the proportion of correct movements with each increase in the number of changes in wheel direction. If β_1 is positive, it means that moving from the reference group (i.e. Group 0: no changes in wheel direction) to the following group (i.e. Group 1: one change in wheel direction) improves accuracy.

3. **Contrast effect** ($\beta_2 Contrast_{ij}$): This term indicates how the proportion of correct movements changes with each incremental increase in contrast. A positive β_2 means that higher contrast leads to a higher proportion of correct movements.

4. **Interaction effect** ($\beta_3 Group_{ij} \cdot Contrast_{ij}$): This term represents how the effect of the number of changes in wheel direction on performance differs between contrast levels. If $\beta_3 > 0$, it suggests that the effect of wiggles on accuracy becomes stronger as the contrast level changes. If $\beta_3 < 0$, it indicates that effect of wiggles on accuracy becomes weaker as the contrast level changes. If $\beta_3 = 0$, it means that there is no interaction, and the effects of wiggle and contrast level are additive and independent of each other.

5. **Random effect** (u_j): This term represents the random variability due to group j. This represents the inter-laboratory variance that is not explained by the fixed effects.

6. **Residual error** (ϵ_{ij}): This term captures the unexplained variability in the model for observation i in group j. It accounts for individual differences in performance that are not explained by the fixed effects (different numbers of changes in wheel direction and contrast levels) and random effects (different laboratories).

The model assumes: (1) random effects (such as variability across laboratories) are normally distributed and (2) observations are independent, which means that individual mice are treated as independent samples. Given the large sample size, these assumptions are reasonable.

Regression Slope Analysis

To assess if the observed linear relationship between temporal frequency and accuracy was statistically significant (**Figure 4**), we performed a shuffle control. We permuted the accuracy values across trials $1,000$ times, each time re-computing the median accuracy per temporal frequency bin and fitting a line to these medians. This yielded a null distribution of slopes expected by chance. We then compared the slope of the original (unshuffled) data to this null distribution to compute a p-value. The p-value represents the proportion of shuffled slopes greater than or equal to the observed slope (one-sided test). This approach tests whether the increase in accuracy with temporal frequency exceeds that expected by chance.

4.2.8 Generalized linear model analysis

We used a binomial generalized linear model to quantify the probability of wiggles as a function of trial history, block congruence, and visual stimulus contrast. We let $Y_i \in \{0, 1\}$ indicate whether trial i was a wiggle, and modeled the probability of wiggles as a log-odds ratio:

$$\log\left(\frac{P\left(Y_i = 1\right)}{1 - P\left(Y_i = 1\right)}\right) = \beta_0 + \beta_1 prev_correct_i + \beta_2 congruent_i + \beta_3 abs_contrast_i + \beta_4 \left(prev_correct_i \times congruent_i\right) \tag{7}$$

In this equation, $prev_correct_i$ was 1 if the previous trial was correct and 0 otherwise; $congruent_i$ was 1 if the visual stimulus side was congruent with the current biased block (right stimulus in right 20% block and left stimulus in left 80% block) and 0 otherwise; $abs_contrast_i$ was the unsigned visual stimulus contrast.

4.2.9 Decoder analysis

The logistic regression decoder maps the input neural activity to the probability of a binary outcome (i.e. left or right stimulus):

$$P\left(stimulus = right \mid x\right) = \frac{1}{1 + e^{-\beta_0 + \sum_{i=1}^{n} \beta_i x_i}} \tag{8}$$

$x = [x_1, x_2, \ldots, x_n]$ is the input vector containing neural activity. For $[0, 0.2]$ seconds of data with a bin size of 0.02 seconds, there are $n = 10$ time bins. Each x_i represents the neural activity in one time bin.

β_0 intercept term of the logistic regression

β_i weight associated with the ith time bin, indicating how strongly the activity in that time bin contributes to predicting choice

$P\left(stimulus = right \mid x\right)$ probability of the right choice given the neural activity

The decoder output is binary:

- Right if $P\left(stimulus = right \mid x\right) > 0.5$
- Left otherwise

The weights $(\beta_0, \beta_1, \ldots, \beta_n)$ are learned during model training by fitting the logistic regression model to maximize the likelihood of observed data (choices). For K trials, the likelihood function is:

$$\mathcal{L}\left(\beta\right) = \prod_{i=1}^{K} P\left(y_i \mid x_i, \beta\right)$$

$y_i \in \{0, 1\}$ stimulus side for trial i (i.e. left $= 0$ and right $= 1$)

x_i neural activity for trial i

$P(y_i = 1 \mid x_i, \beta) = \frac{1}{1+e^{-(\beta_0 + x_i \cdot \beta)}}$ logistic regression equation for probability of the correct stimulus side given the neural activity

Since it is easier to manipulate data as sums rather than products (i.e. for taking derivatives), we use the log-likelihood function:

$$\ell(\beta) = \sum_{i=1}^{N} \left[y_i \log P(y_i \mid x_i, \beta) + (1 - y_i) \log (1 - P(y_i \mid x_i, \beta)) \right] \tag{9}$$

We can substitute the logistic function in Equation 8:

$$P(y_i \mid x_i, \beta) = \frac{1}{1 + e^{-(\beta_0 + x_i \cdot \beta)}}$$

$$\ell(\beta) = \sum_{i=1}^{N} \left[y_i \log \left(\frac{1}{1 + e^{-(\beta_0 + x_i \cdot \beta)}} \right) + (1 - y_i) \log \left(1 - \frac{1}{1 + e^{-(\beta_0 + x_i \cdot \beta)}} \right) \right]$$

$$\ell(\beta) = \sum_{i=1}^{N} \left[y_i (\beta_0 + x_i \cdot \beta) - \log \left(1 + e^{-(\beta_0 + x_i \cdot \beta)} \right) \right]$$

The optimal parameters for $\beta = [\beta_1, \beta_2, \ldots, \beta_n]$ are found by maximizing the log-likelihood function. The goal is to obtain weights for a logistic regression model that produces probabilities aligned with the observed data.

4.2.10 Computation of Temporal Contrast Sensitivity

A behavioral d' was used to measure temporal contrast sensitivity (TCS):

$$d' = z(Hit) - z(FA) \tag{10}$$

$z(Hit)$ z-score of the probability of hits

$z(FA)$ z-score of the probability of false slarms

Temporal contrast sensitivity is a function of temporal frequency, spatial frequency, and background mean illumination (screen brightness). Screen brightness was not well-standardized across laboratories and no published value for illumination is listed (The International Brain Laboratory, 2021). On average, we determined that the screen brightness was 29.4 cd m^{-2}. This means that $\log(29.4) = 1.47$ log cd m^{-2}. Therefore, we used the data under photopic (1.80 log cd m^{-2}) conditions (See **Figure 2b** of Umino et al, 2008; **Figure 6f** of Umino et al, 2018) for details of mouse temporal contrast sensitivity analysis).

visual stimulus properties	The International Brain Laboratory, 2021	Umino et al, 2018
size	local	full field
contrast	6.25%	50%
spatial frequency	0.1 cycles per degree	0.128 cycles per degree
brightness	1.47 log cd m^{-2}	1.80 log cd m^{-2}

Table 4: These are caveats in the interpretation of mouse temporal contrast sensitivity.

Data Availability

Please follow these instructions to download the data. There are visualizations available to understand the data (Birman et al, 2024).

Code Availability

Please visit our Github repository to access the code used to produce the main results and figures presented in this manuscript. This International Brain Lab Github repository also contains code for brain-wide neural data analysis.

Acknowledgements

This work was supported by the Gatsby Charitable Foundation (GAT3755). Computational resources were provided by University College London. We thank the Kavli Institute of Theoretical Physics for providing the environment to see this paper to completion (NSF PHY-2309135). We thank Thomas Mrsic-Flogel, Peter Latham, and David Kleinfeld for comments on the behavioral and neural data analysis. We thank Anne Churchland, Andrew Peters, Viktor Roytman, and Alvin Zhang for comments on the manuscript. We are especially grateful to Laurence F. Abbott and Peter Dayan for inspection of the data and text.

5 References

[1] Ayaz, A., Saleem, A. B., Schölvinck, M. L., & Carandini, M. (2013). Locomotion controls spatial integration in mouse visual cortex. Current Biology, 23(10), 890-894.

[2] Birman, D., Chapuis, G., Faulkner, M., Rossant, C., Laboratory, I. B., Benson, J., ... & Winter, O. (2024). Interactive data exploration websites for large-scale electrophysiology. bioRxiv.

[3] Born, J. (2009). Active Sensing [PowerPoint slides]. Harvard University. https://www.hms.harvard.edu/bss/neuro/bo sensing.pdf

[4] Bouvier, G., Senzai, Y., & Scanziani, M. (2020). Head movements control the activity of primary visual cortex in a luminance-dependent manner. Neuron, 108(3), 500-511.

[5] Dadarlat, M. C., & Stryker, M. P. (2017). Locomotion enhances neural encoding of visual stimuli in mouse V1. Journal of Neuroscience, 37(14), 3764-3775.

[6] De Valois, R. L., Albrecht, D. G., & Thorell, L. G. (1982). Spatial frequency selectivity of cells in macaque visual cortex. Vision research, 22(5), 545-559.

[7] Dipoppa, M., Ranson, A., Krumin, M., Pachitariu, M., Carandini, M., & Harris, K. D. (2018). Vision and locomotion shape the interactions between neuron types in mouse visual cortex. Neuron, 98(3), 602-615.

[8] Fenk, L. M., Avritzer, S. C., Weisman, J. L., Nair, A., Randt, L. D., Mohren, T. L., ... & Maimon, G. (2022). Muscles that move the retina augment compound eye vision in Drosophila. Nature, 612(7938), 116-122.

[9] Findling, C., Hubert, F., International Brain Laboratory, Acerbi, L., Benson, B., Benson, J., ... & Pouget, A. (2023). Brain-wide representations of prior information in mouse decision-making. BioRxiv, 2023-07.

[10] Fulvio, J. M., Miao, H., & Rokers, B. (2021). Head jitter enhances three-dimensional motion perception. Journal of vision, 21(3), 12. https://doi.org/10.1167/jov.21.3.12

[11] Green, L., Tingley, D., Rinzel, J., & Buzsáki, G. (2022). Action-driven remapping of hippocampal neuronal populations in jumping rats. Proceedings of the National Academy of Sciences, 119(26), e2122141119.

[12] Guitchounts, G., Masís, J., Wolff, S. B., & Cox, D. (2020). Encoding of 3D head orienting movements in the primary visual cortex. Neuron, 108(3), 512-525.

[13] Gulbinaite, R., Nazari, M., Rule, M. E., Bermudez-Contreras, E. J., Cohen, M. X., Mohajerani, M. H., & Heimel, J. A. (2024). Spatiotemporal resonance in mouse primary visual cortex. Current Biology, 34(18), 4184-4196.

[14] Gupta, D., DePasquale, B., Kopec, C. D., & Brody, C. D. (2024). Trial-history biases in evidence accumulation can give rise to apparent lapses in decision-making. Nature communications, 15(1), 662.

[15] Han, X., & Bonin, V. (2024). Higher-order cortical and thalamic pathways shape visual processing streams in the mouse cortex. Current Biology, 34(24), 5671-5684.

[16] Huang, X., Ghimire, B., Chakrala, A. S., & Wiesner, S. (2023). Neural encoding of multiple motion speeds in visual cortical area MT. BioRxiv.

[17] International Brain Laboratory, Aguillon-Rodriguez, V., Angelaki, D., Bayer, H., Bonacchi, N., Carandini, M., ... & Zador, A. M. (2021). Standardized and reproducible measurement of decision-making in mice. Elife, 10, e63711.

[18] International Brain Laboratory, Benson, B., Benson, J., Birman, D., Bonacchi, N., Bougrova, K., ... & Witten, I. B. (2023). A brain-wide map of neural activity during complex behavior. biorxiv, 2023-07.

[19] Intoy, J., & Rucci, M. (2020). Finely tuned eye movements enhance visual acuity. Nature communications, 11(1), 795.

[20] Keller, G. B., Bonhoeffer, T., & Hübener, M. (2012). Sensorimotor mismatch signals in primary visual cortex of the behaving mouse. Neuron, 74(5), 809-815.

[21] Kelly, D. H. (1979). Motion and vision. I. Stabilized images of stationary gratings. Journal of the Optical Society of America, 69(9), 1266-1274.

[22] Kato, S., Kaplan, H. S., Schrödel, T., Skora, S., Lindsay, T. H., Yemini, E., ... & Zimmer, M. (2015). Global brain dynamics embed the motor command sequence of Caenorhabditis elegans. Cell, 163(3), 656-669.

[23] King, C. W., Ledochowitsch, P., Buice, M. A., & de Vries, S. E. (2023). Saccade-responsive visual cortical neurons do not exhibit distinct visual response properties. Eneuro, 10(9).

[24] Kurnikova, A., Moore, J. D., Liao, S. M., Deschênes, M., & Kleinfeld, D. (2017). Coordination of orofacial motor actions into exploratory behavior by rat. Current Biology, 27(5), 688-696.

[25] Liao, S. M., & Kleinfeld, D. (2023). A change in behavioral state switches the pattern of motor output that underlies rhythmic head and orofacial movements. Current Biology, 33(10), 1951-1966.

[26] Marshel, J. H., Garrett, M. E., Nauhaus, I., & Callaway, E. M. (2011). Functional specialization of seven mouse visual cortical areas. Neuron, 72(6), 1040-1054.

[27] Meyer, A. F., Poort, J., O'Keefe, J., Sahani, M., & Linden, J. F. (2018). A head-mounted camera system integrates detailed behavioral monitoring with multichannel electrophysiology in freely moving mice. Neuron, 100(1), 46-60.

[28] Millman, D. J., Ocker, G. K., Caldejon, S., Kato, I., Larkin, J. D., Lee, E. K., ... & de Vries, S. E. (2020). VIP interneurons in mouse primary visual cortex selectively enhance responses to weak but specific stimuli. Elife, 9, e55130.

[29] Mitchell, J. F., Reynolds, J. H., & Miller, C. T. (2014). Active vision in marmosets: a model system for visual neuroscience. Journal of Neuroscience, 34(4), 1183-1194.

[30] Miura, S. K., & Scanziani, M. (2022). Distinguishing externally from saccade-induced motion in visual cortex. Nature, 610(7930), 135-142.

[31] Monavarfeshani, A., Sabbagh, U., & Fox, M. A. (2017). Not a one-trick pony: Diverse connectivity and functions of the rodent lateral geniculate complex. Visual neuroscience, 34, E012.

[32] Murakami, I., & Cavanagh, P. (1998). A jitter after-effect reveals motion-based stabilization of vision. Nature, 395(6704), 798-801.

[33] Murray, P. D., Masri, R., & Keller, A. (2010). Abnormal anterior pretectal nucleus activity contributes to central pain syndrome. Journal of Neurophysiology, 103(6), 3044-3053.

[34] Musall, S., Kaufman, M. T., Juavinett, A. L., Gluf, S., & Churchland, A. K. (2019). Single-trial neural dynamics are dominated by richly varied movements. Nature neuroscience, 22(10), 1677-1686.

[35] Niell, C. M., & Stryker, M. P. (2010). Modulation of visual responses by behavioral state in mouse visual cortex. Neuron, 65(4), 472-479.

[36] Palmisano, S., Pinniger, G. J., Ash, A., & Steele, J. R. (2009). Effects of simulated viewpoint jitter on visually induced postural sway. Perception, 38(3), 442-453.

[37] Parker, P. R., Abe, E. T., Leonard, E. S., Martins, D. M., & Niell, C. M. (2022). Joint coding of visual input and eye/head position in V1 of freely moving mice. Neuron, 110(23), 3897-3906.

[38] Prins, N. (2012). The psychometric function: The lapse rate revisited. Journal of Vision, 12(6), Article 25. https://doi.org/10.1167/12.6.25

[39] Ranade, S., Hangya, B., & Kepecs, A. (2013). Multiple modes of phase locking between sniffing and whisking during active exploration. Journal of Neuroscience, 33(19), 8250-8256.

[40] Rees, H., & Roberts, M. H. T. (1993). The anterior pretectal nucleus: a proposed role in sensory processing. Pain, 53(2), 121-135.

[41] Rolfs, M., Schweitzer, R., Castet, E., Watson, T. L., & Ohl, S. (2023). Lawful kinematics link eye movements to the limits of high-speed perception. bioRxiv, 2023-07.

[42] Roy, S., Bohlen, M. O., Cruger, J., Kuczewski, G., Shultz, N., Fitzpatrick, D., ... & Field, G. (2025). Characterization of retinal ganglion cells projecting to the superior colliculus in tree shrew. Investigative Ophthalmology & Visual Science, 66(8), 3339-3339.

[43] Rucci, M., Iovin, R., Poletti, M., & Santini, F. (2007). Miniature eye movements enhance fine spatial detail. Nature, 447(7146), 852-855.

[44] Saleem, A. B., Ayaz, A., Jeffery, K. J., Harris, K. D., & Carandini, M. (2013). Integration of visual motion and locomotion in mouse visual cortex. Nature neuroscience, 16(12), 1864-1869.

[45] Singh, V. P., Li, J., Dawson, K., Mitchell, J. F., & Miller, C. T. (2025). Active vision in freely moving marmosets using head-mounted eye tracking. Proceedings of the National Academy of Sciences, 122(6), e2412954122.

[46] Skyberg, R. J., & Niell, C. M. (2024). Natural visual behavior and active sensing in the mouse. Current Opinion in Neurobiology, 86, 102882.

[47] Stringer, C., Pachitariu, M., Steinmetz, N., Reddy, C. B., Carandini, M., & Harris, K. D. (2019). Spontaneous behaviors drive multidimensional, brainwide activity. Science, 364(6437), eaav7893.

[48] Tinbergen, N. (1974). Ethology and stress diseases. Science, 185(4145), 20-27.

[49] Umino, Y., Pasquale, R., & Solessio, E. (2018). Visual temporal contrast sensitivity in the behaving mouse shares fundamental properties with human psychophysics. Eneuro, 5(4).

[50] Wang, Z. J., Melfi Jr, J., & Leonardo, A. (2022). Recovery mechanisms in the dragonfly righting reflex. Science, 376(6594), 754-758.

[51] Watson, L. M., Strang, N. C., Scobie, F., Love, G. D., Seidel, D., & Manahilov, V. (2012). Image jitter enhances visual performance when spatial resolution is impaired. Investigative Ophthalmology & Visual Science, 53(10), 6004-6010.

[52] Xiao, W., Sharma, S., Kreiman, G., & Livingstone, M. S. (2024). Feature-selective responses in macaque visual cortex follow eye movements during natural vision. Nature neuroscience, 27(6), 1157-1166.

[53] Zhao, Z., Ahissar, E., Victor, J. D., & Rucci, M. (2023). Inferring visual space from ultra-fine extra-retinal knowledge of gaze position. Nature communications, 14(1), 269.

[54] Zhaoping, L. (2019). A new framework for understanding vision from the perspective of the primary visual cortex. Current opinion in neurobiology, 58, 1-10.